Emergent Materials (2021) 4:1441–1453
https://doi.org/10.1007/s42247-021-00282-7

ORIGINAL ARTICLE

Pyrite (FeS_2)-supported ultrafiltration system for removal of mercury (II) from water

Dong Suk Han[1] · Kawsher M. D. Solayman[2] · Ho Kyong Shon[3] · Ahmed Abdel-Wahab[2]

Received: 16 February 2021 / Accepted: 21 July 2021 / Published online: 13 August 2021

Abstract

This study investigated the Hg(II) removal efficiencies of the reactive adsorbent membrane (RAM) hybrid filtration process, a removal process that produces stable final residuals. The reaction mechanism between Hg(II) and pyrite and the rejection of the solids over time were characterized with respect to flux decline, pH change, and Hg and Fe concentration in permeate water. Effects of the presence of anions (Cl^-, SO_4^{2-}, NO_3^-) or humic acid (HA) on the rejection of the Hg(II)-contacted pyrite were studied. The presence of both HA and Hg(II) increased the rate of flux decline due to the formation of irreversible gel-like compact cake layers as shown in the experimental data and modeling related to the flux decline and the SEM images. Stability experiments of the final residuals retained on the membrane using a thiosulfate solution ($Na_2S_2O_3$) show that the Hg(II)-laden solids were very stable due to little or no detection of Hg(II) in the permeate water. Experiment on the possibility of continuously removing Hg(II) by reusing the Hg/pyrite-laden membrane shows that almost all Hg(II) was adsorbed onto the pyrite surface regardless of the presence of salts or HA, and the Hg(II)-contacted pyrite residuals were completely rejected by the DE/UF system. Therefore, a membrane filter containing pyrite-Hg(II) could provide another reactive cake layer capable of further removal of Hg(II) without post-chemical treatment for reuse.

Keywords Pyrite · Mercury · Adsorption · Ultrafiltration · Dead-end flow

1 Introduction

Mercury (Hg) is a global contaminant and of significant concern for centuries. This is due to its high toxicity and bioaccumulation via the aquatic food chain, which seriously affects natural ecosystems and human health. Various treatment processes for mercury (II) removal from water have been used, such as adsorption [1–8], filtration [9, 10], precipitation/co-precipitation [11], ion exchange [12], and bioremediation [13]. Limitations encountered in the application of these methods include slow kinetics and incomplete removal, production of large amounts of Hg(II)-contaminated sludge, metallic fouling of ion exchange media, membrane fouling, and fairly high operating costs. Moreover, the presence of natural organic matter (NOM) [4, 14–18] and background ions [4, 10] or co-existing metal ions (Mg^{2+}, Mn^{2+}, and Cu^{2+}) [4] affect mercury removal by these treatment methods. Therefore, enhanced technologies are required to remove mercury efficiently from water while producing stable residuals that can be effectively separated from water and then safely disposed to landfills.

A new process called reactive adsorbent/membrane (RAM) is a hybrid filtration process that has shown promise to attain high quality water from wastewater or water resources contaminated with Hg(II) [9, 10, 19]. This method is based on the sorption of Hg(II) by a reactive adsorbent, which is subsequently separated from water by an ultrafiltration membrane in a continuous flow way. Mercury is a Lewis acid that has a strong affinity to soft Lewis bases. Since the thiol functional group is a soft base, sulfur-containing chemicals have been widely used to remove mercury from water [2, 3, 8, 20, 21]. Accordingly, mercury forms very

✉ Dong Suk Han
dhan@qu.edu.qa

✉ Ahmed Abdel-Wahab
ahmed.abdel-wahab@qatar.tamu.edu

1 Center for Advanced Materials & Department of Chemical Engineering, Qatar University, Doha, Qatar

2 Chemical Engineering Program, Texas A&M University At Qatar, Doha, Qatar

3 Centre for Technology in Water and Wastewater (CTWW), School of Civil and Environmental Engineering, University of Technology (UTS), Ultimo, NSW, Australia

insoluble solids with sulfide [22, 23]. The most common sulfide/disulfide minerals are pyrite (FeS_2), mackinawite (FeS), and pyrrhotite ($Fe_{1-x}S$, x = 0 to 0.2). The abundance of pyrite on the earth surface and its low cost led many environmental engineers and researchers to use them as possible scavengers of many toxic elements including mercury [8, 24–26]. Therefore, an attractive alternative for effective mercury removal is to adopt pyrite as a reactive adsorbent for Hg(II), possibly producing stable residuals that can be effectively separated by ultrafiltration membranes. Pyrite can adsorb Hg(II) effectively over a wide range of pH [3, 8]. In most previous studies, the mechanism for adsorption of mercury and the species formed have not been fully understood. However, several potential mechanisms may occur during removal of Hg by pyrite: formation of hydrolyzed Hg species which subsequently adsorbed onto the pyrite surface and formation of new a solid-phase through ion exchange between Hg(II) and the Fe in pyrite [22].

Even though Hg is strongly adsorbed onto pyrite surfaces, desorption of Hg from Hg-contacted pyrite is possible when strong ligands, such as I^-, $S_2O_3^{2-}$, and CN^-, that have a high affinity to Hg(II) species, are present in the solution [27]. Also the presence of dissolved organic matter (DOM) and some complexing anions may negatively affect Hg sorption onto pyrite [10, 17]. Anions such as Cl^- and SO_4^{2-} may decrease the sorption of mercury by forming strong non-sorbing aqueous complexes [28], thus reducing free Hg(II) ions available to sorb onto the surface of sorbent. In addition, complexation between mercury and DOM [15, 16, 29–31], adsorption of humic acid (HA) on the surface of pyrite [32], and the competition between organic S of DOM and inorganic S of pyrite for complexation with Hg [17] may influence the adsorption of Hg onto pyrite. Moreover, pyrite oxidation either by dissolved oxygen in aqueous media or redox reaction between Hg(II) and structural Fe of pyrite may strongly influence the sorption behavior of Hg onto pyrite [2].

On the other hand, the separation of Hg-contacted solid is a technological challenge. Ultrafiltration (UF), nanofiltration (NF), and reverse osmosis (RO) are capable of reducing concentrations of Hg-containing solids after appropriate pretreatment [9, 10, 33–35]. However, UF processes is preferred, because they can achieve the goal at lower operating pressure, which reduces the capital and operating costs [33, 36]. Appropriate pretreatment and choice of membrane and operation conditions are needed to reach highest removal efficiency of contaminants.

The objective of this study was to develop a RAM treatment process for removal of Hg from wastewater that forms stable solid residuals. Nano-scale pyrite was used as a reactive sorbent at pH 8 and was combined with DE/UF to separate the Hg-loaded residuals from treated wastewater. Effects of the presence of anions (Cl^-, SO_4^{2-}, NO_3^-) and humic acid (HA, as example of NOM) on Hg(II) removal were studied, and the stability of final residuals rejected by the DE-UF was evaluated by using thiosulfate solution ($Na_2S_2O_3$) as a desorbing reagent. Most of the previous mercury removal experiments were batch experiments. This study examined the possibility of continuous removal of Hg(II) by formation of Hg-pyrite followed by its removal by DE/UF. Moreover, this study also investigated the possible reaction mechanism between Hg(II) and pyrite and characterized the final solid residual by surface analysis techniques including scanning electron microscopy (SEM) and X-ray photoelectron spectroscopy (XPS). The fouling mechanism was investigated by nonlinear regression analysis using MATLAB and SEM analysis.

2 Materials and methods

2.1 Chemicals

All materials and chemicals used in this research were reagent grade. Water was distilled by a Barnstead Mega-pure distillation device and then deionized by passing it through a Labconco purifier system. Subsequently, the distilled/deionized water was purged with 99.99% N_2 to produce deoxygenated, deionized water (DDW). All stock solutions and chemical reagents used in this study were prepared by dissolving these high quality chemicals with DDW in anaerobic chamber with an atmosphere of 99.99% nitrogen. Also, all experiments were conducted in an anaerobic atmosphere.

Iron (III) chloride hexahydrate ($FeCl_3{\cdot}6H_2O$, Sigma-Aldrich, 97%) and sodium sulfide nonahydrate ($Na_2S{\cdot}9H_2O$, Sigma-Aldrich, 99.9%) were used as iron and sulfur sources, respectively, to synthesize pyrite. Mercury stock solutions were prepared using mercuric chloride ($HgCl_2$) obtained from Mallinckrodt Chemicals, Phillipsburg, NJ. Anhydrous sodium sulfate (Na_2SO_4, BDH), sodium chloride (NaCl, Fisher Scientific), and sodium nitrate ($NaNO_3$, Sigma-Aldrich) were used as source of anions. Humic acid (HA) was purchased from Sigma-Aldrich and used to represent natural organic matter. Anhydrous sodium thiosulfate ($Na_2S_2O_3$) was purchased from AMRESCO for desorption tests of Hg(II). All the solutions used in experiments were adjusted to pH 8.0 ± 0.1 using 0.1 M NaOH and 0.1 M HCl (J. T. Baker). The pH was monitored with a Thermo Scientific pH meter calibrated with three Orion buffer solutions (4.0, 7.0, and 10).

2.2 Pyrite synthesis

Pyrite (FeS_2) was synthesized in an anaerobic chamber using a modified method of Kim et al. [37], which used $Na_2S{\cdot}9H_2O$ and $FeCl_3{\cdot}6H_2O$ as sources of sulfur and iron.

pH was adjusted to 6.5, which is the optimum pH to avoid the possible formation of FeS and S^0 [38]. The pyrite synthesized in our laboratory was characterized by surface analysis. The detailed procedure for pyrite synthesis is described in the Supporting Information. SEM/EDX analysis showed that the mass percentage of synthesized pyrite was 83% (Fig. S1). Average particle size of synthesized pyrite was around 400 nm.

2.3 Dead-end ultrafiltration system

A dead-end ultrafiltration (DE/UF) membrane system was setup with a low pressure, stirred-cell UF device provided by Millipore Company (Fig. 1). This device consisted of an 800-mL glass reservoir container connected to a 300-mL glass cell that held the membrane. Pressure was maintained at 14.5 psi by a pressure regulator connected to a N_2

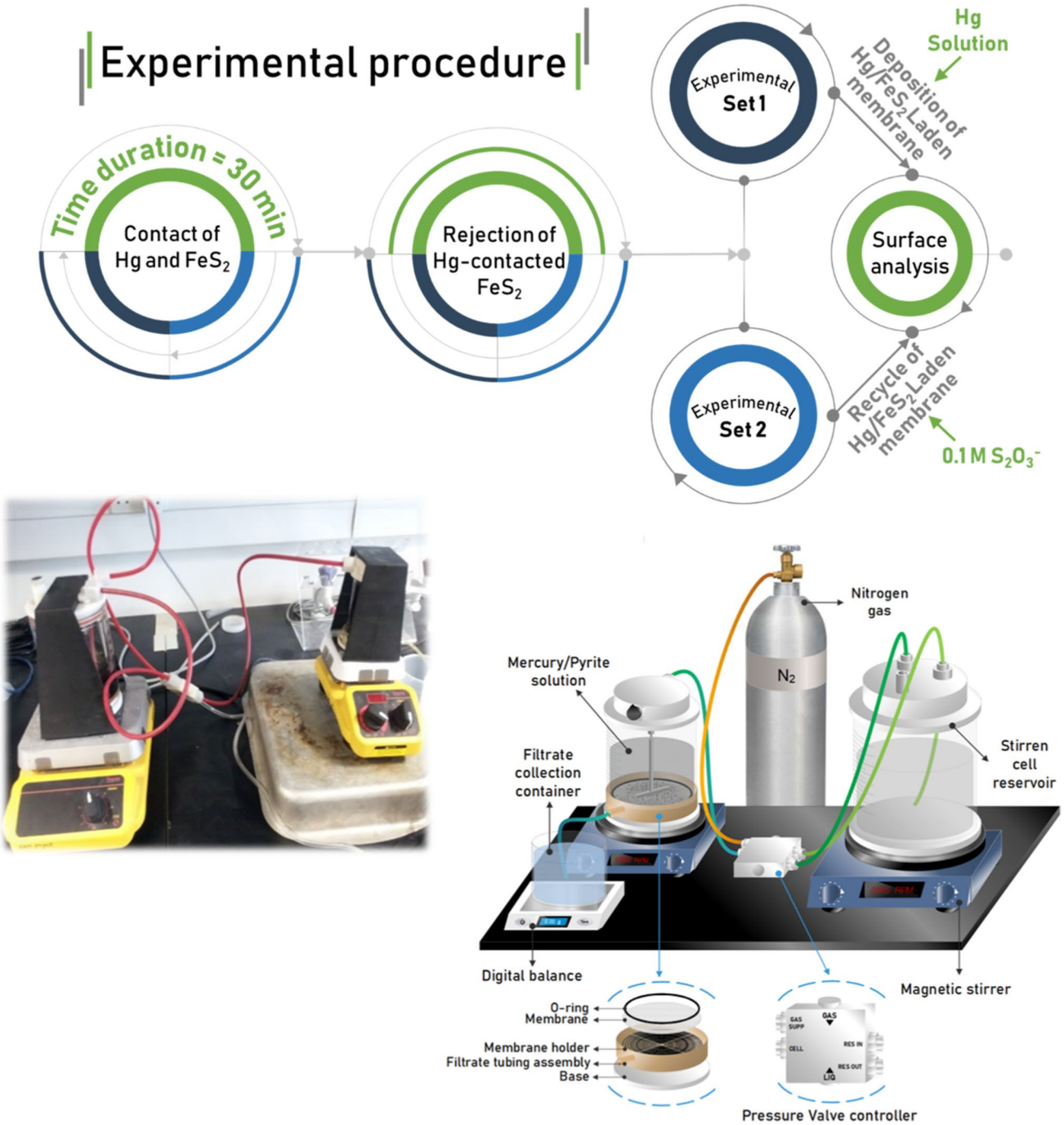

Fig. 1 Schematic representation and flow chart of experimental procedures for mercury removal using dead-end ultrafiltration membrane system

cylinder. Membrane used for the DE/UF system was 30 kDa regenerated cellulose (RC) UF membrane with surface area of 31.7 cm^2. There was no Hg(II) adsorption on the walls of the DE/UF system when the control test was conducted with only a mercury solution.

2.4 Mercury removal using DE/UF system

A series of filtration experiments were conducted with two sets including several steps. These sets were categorized by the presence of desorption test. So, set I follows experimental order of sorption → rejection → recycle, whereas set II has the order sorption → rejection → desorption. These two set experiments were performed separately. For step I in set I (sorption test), pyrite was contacted with the water containing Hg(II) for 30 min. In step II (rejection test), the ability of the ultrafiltration membrane to reject Hg(II)-laden pyrite was determined. In step III (recycle test), the ability of the Hg(II)-laden pyrite on the membrane to remove additional Hg(II) was determined by passing water containing Hg(II) through the membrane. On the other hand, the set II experiment has a desorption test after a rejection test without recycle test.

Regardless of the set type, in each step except step I, permeate water was collected over time in order to measure flux, pH, and concentrations of Hg and Fe. These results were used to obtain removal efficiencies and to identify the possible reaction mechanism, the fouling propensity of membrane, and the overall retention capacity of the ultrafiltration system. The setup of the DE/UF system is schematically represented in Fig. 1.

For the rejection test (step II), a feed solution of 1 mg/L Hg(II) and 0.1 g/L pyrite was prepared by mixing equal volumes of a 0.2 g/L pyrite suspension and a 2 mg/L Hg(II) solution. Although mercury concentrations in natural water have been reported to range as low as several µg/L [39], a higher concentration of Hg(II) was chosen in this experiment to evaluate the efficiencies of our system for mercury removal from wastewaters. Since the maximum sorption capacity of pyrite for mercury was found to be 9.9 mg Hg/g [4], a pyrite concentration of 0.1 g/L is appropriate for these filtration experiments. In addition, pH higher than neutral has been reported to be favorable for efficient and rapid removal of mercury by pyrite [3, 4]. Moreover, Hg-chloro complexes predominate at pH less than 8, which might be unfavorable for adsorption of mercury onto pyrite [3, 4]. Therefore, pH of all solutions was adjusted to 8.0 ± 0.1 by deoxygenated NaOH and HCl solutions.

For the evaluation of physical and chemical stability of the rejected final solids on the UF membrane (step III in set II), a 0.1 M thiosulfate ($S_2O_3^{2-}$) solution was continuously passed through the membrane.

To study the effect of anions (SO_4^{2-}, NO_3^{2-}, and Cl^-) on the behavior of Hg(II) removal by pyrite and the rejection of Hg-laden pyrite by the DE/UF system, experiments were conducted in the presence of 0.01 M SO_4^{2-}, NO_3^{2-}, and Cl^-. Anions were reported to significantly affect the sorption behavior of Hg and other heavy metals by pyrite [4]. Although the reported values of anions in the environment are very low, high concentration of anions were chosen in this study to evaluate the efficiencies of our system for Hg(II) removal from wastewater under adverse conditions. To study the effect of NOM on filtration experiments, HA was used as a representative of NOM at two concentrations (1 mg/L and 0.2 mg/L). HA can reduce the adsorption of Hg(II) onto pyrite by competing with Hg(II) for active sites of pyrite and subsequently passivating pyrite surface by reversible and irreversible adsorption of HA [40]. At low ratios of HA to Hg, Hg(II) can be reduced to Hg(0) by HA. However, as the concentration of HA increases, the formation of Hg-Ha complexes becomes more important, and at very high HA concentration, complexation completely eliminates reduction [31].

2.5 Surface characterization of solid samples and membranes

The surfaces of solid samples were characterized using techniques, including SEM for the surface topography and composition and XPS for identification and quantification of elemental composition. Prior to SEM analysis, the membranes were coated with gold alloy through a vacuum-sputtering technique to prevent the accumulation of electrostatic charge at the surface. Otherwise, scanning faults or low resolution of backscattering SEM images could occur. The secondary SEM images were collected at a working distance of 10 mm under an acceleration voltage of 20–25 kV. Image magnification ranged from 200 to 80,000×. The quantification of elemental composition on the solid was carried out using a Kratos Axis Ultra DLD XPS. The XPS spectra were obtained using a monochromatic Al Kα X-rays with pass energy of 80 eV.

3 Results and discussion

3.1 Rejection of Hg-contacted pyrite

Figure 2a shows flux decline during four different experiments. Each experiment showed flux decline due to membrane fouling, possibly caused by pore constriction, pore blocking, or formation of a cake layer by deposition of particles on the surface [41]. To evaluate the actual fouling mechanism, a flux model proposed in the literatures is used [9, 41]:

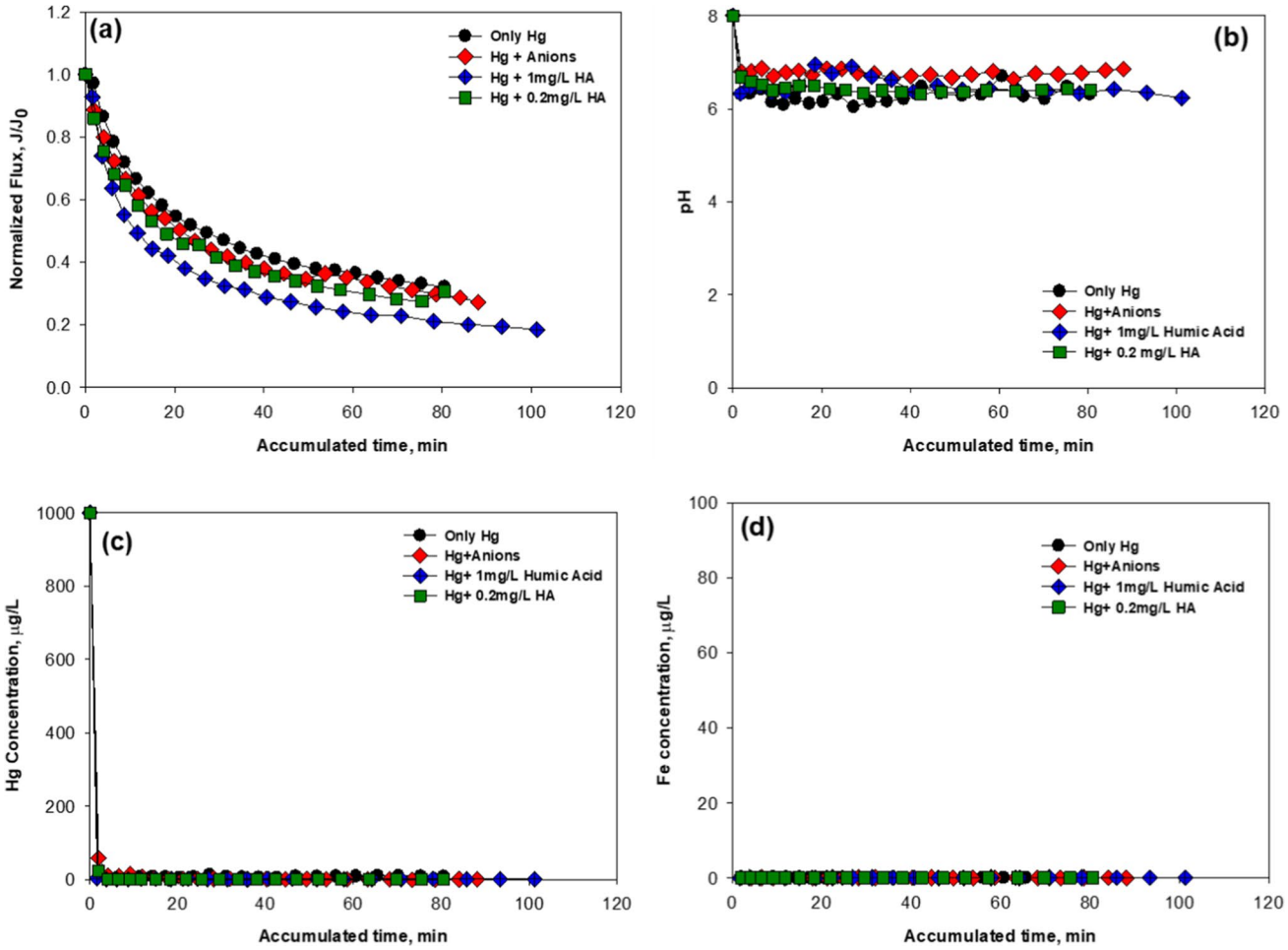

Fig. 2 **a** Flux decline of Hg(II)-contacted pyrite suspension using DE/UF system as affected by anions and HA; time-profiled **b** pH, **c** Hg, and **d** Fe concentrations in the same permeate water: 0.1 g/L pyrite, 1 mg/L Hg(II), 14.5 psi pressure, initial flow rate of 3.54 Lm^{-3} min^{-1}, pH 8, 10 mM anions (Cl^-, SO_4^{2-}, NO_3^-), 0.2 and 1 mg/L HA, and N_2-purged system

$$J = J_0(1 + kt)^{-n} \quad (1)$$

where J is the flux at a given time t, J_0 is the initial flux, k is an empirical rate constant, and n is a coefficient determined by the fouling mechanism. When the value of n is 0.5, 1, 1.5, or 2, it indicates that flux decline is due to the cake formation, internal pore constriction, partial pore blocking, or complete pore blocking, respectively. In this study, values of the rate constant (k) were determined by nonlinear regression using the "nlinfit" function in MATLAB. Regressions were conducted with each of the four values of n. The sum of squared residuals (SSR) is a measure of the goodness of fit. Table 1 shows that the lowest SSR was always observed when the value of n was set to 0.5, which indicates that the cake formation model provided the best fit to the flux decline data. The detailed fitting results are presented in the Supporting Information (Figs. S2–S5). In addition, the presence of HA resulted in more rapid fouling as indicated by

Table 1 Calculated parameters of the flux decline model for rejection of pyrite and Hg(II)-contacted pyrite under various solution compositions

Samples	SSR[a]/k			
	$n = 0.5$	$n = 1.0$	$n = 1.5$	$n = 2.0$
Pyrite + Hg	0.005/0.111	0.291/0.035	0.057/0.019	0.077/0.013
Pyrite + Hg + anions	0.002/0.139	0.052/0.041	0.097/0.023	0.127/0.016
Pyrite + Hg + 0.2 mg/L HA	0.003/0.165	0.052/0.048	0.094/0.027	0.123/0.018
Pyrite + Hg + 1 mg/L HA	0.009/0.256	0.045/0.069	0.097/0.037	0.135/0.025

[a]SSR is sum of squared residual between experimental data and flux decline model

the larger values of *k*. The presence of both HA and Hg may result in higher rates of flux decline due to the formation of irreversible gel-like compact cake layers [42–44].

Humic substances can form complexes with both Hg(II) [30] and pyrite [40], which ultimately result in macromolecules. Deposition of these larger macromolecules can make a thick cake layer on the membrane. HAs are negatively charged because of the presence of negatively charged carboxylic and phenolic groups, and these results in electrostatic repulsion between molecules of HA. However, complexation of HA with pyrite or with Hg could reduce electrostatic repulsion between HA molecules, and this could help the formation of coiled and spherical shape among them, finally producing a more compact layer on the surface of membrane [43, 45]. This is evident in all cases with HA, but the flux decline is substantial in the case with higher concentration of HA. Similarly, the presence of anions also resulted in slightly greater flux decline as compared to the case with only Hg, possibly because of deposition of the Hg-anion-pyrite solids on the membrane surface. For example, Bower et al. (2008) found an ordered monolayer of Hg-Cl-S on the surface of pyrite based on the EXAFS data, in which linear S-Hg-Cl arrangements seems to be extended away from one of the S atoms in 50% of the disulfide pairs at the pyrite (001) surface [3]. These Hg-anion-pyrite solids could make the cake layer denser and thicker.

pH and concentrations of Hg and Fe in the permeate water were also measured. Figure 2b shows that the influent pH of 8 decreased to effluent pH values between 6 and 7 for all experiments. For the case of Hg only, the decrease of pH is likely due to sorption of Hg-hydroxo complexes onto the pyrite surface, which releases protons into solution [2–4], as shown in Eq. (2):

$$\equiv \mathrm{Py} \cdots \mathrm{OH} + \mathrm{Hg}^{2+} \rightarrow \equiv \mathrm{Py} \cdot \cdot \mathrm{O} \cdot \cdot \mathrm{Hg}^{+} + \mathrm{Hg}^{+} \quad (2)$$

where ≡Py··OH indicates a hydrolyzed pyrite surface. Slightly less pH decrease was observed in the solution in presence of anions comparing to other solutions. This might be due to the complexation between Hg(II) and anions such as Hg-Cl_2, resulting in less free Hg available for formation of Hg-OH^+ or FeS_2-Hg-OH complex [4].

Another explanation for the decrease in pH is oxidation of pyrite by dissolved oxygen. It cannot be ensured that the whole process is completely anoxic condition. During transfer of the feed solutions from glove box to feed water reservoir, the feed solutions were partially exposed to air for brief time. Pyrite oxidation is a complex phenomenon, and both sulfur and iron(II) can be oxidized. Pyritic sulfur can be oxidized to sulfate by dissolved oxygen. But the oxidation of Fe(II) produces Fe(III), which is another oxidizing agent for pyrite, eventually leading to oxidation of pyrite by both oxygen and Fe(III), which increases the acidity of the solution [2–4, 46].

$$\mathrm{FeS_2} + 7/2\mathrm{O_2} + \mathrm{H_2O} = \mathrm{Fe^{2+}} + 2\mathrm{SO_4^{2-}} + 2\mathrm{H^+} \quad (3)$$

$$\mathrm{Fe^{2+}} + 1/4\mathrm{O_2} + \mathrm{H^+} = \mathrm{Fe^{3+}} + 1/2\mathrm{H_2O} \quad (4)$$

$$\mathrm{FeS_2} + 14\mathrm{Fe^{3+}} + 8\mathrm{H_2O} = 15\mathrm{Fe^{2+}} + 2\mathrm{SO_4^{2-}} + 16\mathrm{H^+} \quad (5)$$

In this study, all experiments achieved around 99% removal of Hg (Fig. 2c), indicating that almost all of the mercury was adsorbed onto pyrite particles and that the final solids were completely rejected by ultrafiltration membrane system. The presence of anions or HA did not affect the removal efficiency of the system.

Figure 2d shows that Fe was not detected in the permeate water. The lack of Fe in the permeate water can be explained in two ways: (a) Removal of Hg resulted in formation of HgS that released Fe, but it was re-adsorbed onto the pyrite surface or precipitated as iron (hydr)oxide and (b) removal of Hg did not cause any release of Fe from pyrite. Our experimental methodology cannot distinguish between these two explanations. Considering all of the aspects, adsorption of mercury species onto pyrite surface and the resulting surface complexation seems to be the most plausible removal mechanism for Hg.

Figure 3 shows several pictures of the membrane before and after filtration experiments that had been dried in an anaerobic chamber. The dried membrane surface had a brown-yellow color in all cases, but the yellow color is stronger when HA was present in the solution (Fig. 3e and f). The change in color may be related to the oxidation of membrane surface. Quantitative elemental analysis of the membrane surface by XPS (Fig. S6) shows a high percentage of elemental oxygen in all cases. This could be caused by exposure of the membranes to air during transport to the anaerobic chamber after experiments and during preparation of samples for SEM and XPS analysis, which was conducted outside the anaerobic chamber, or the hydrolyzed surface of the rejected pyrite solids.

Figure 4 shows the top and cross-sectional views of SEM images of membrane surfaces from all experimental conditions. The cross-sectional images (Fig. 4e–h) of the membrane surface show that Hg-contacted pyrite formed a cake layer on the membrane surface. No particles penetrated into the pores of the membrane. Top view images (Fig. 4a–d) show that the cake layer covered the entire area of the membrane surface. This supports the conclusion based on flux decline measurements that cake formation was the dominant fouling mechanism in all cases. The top view images also show that in cases without HA, the fouling layers look relatively porous, whereas in cases

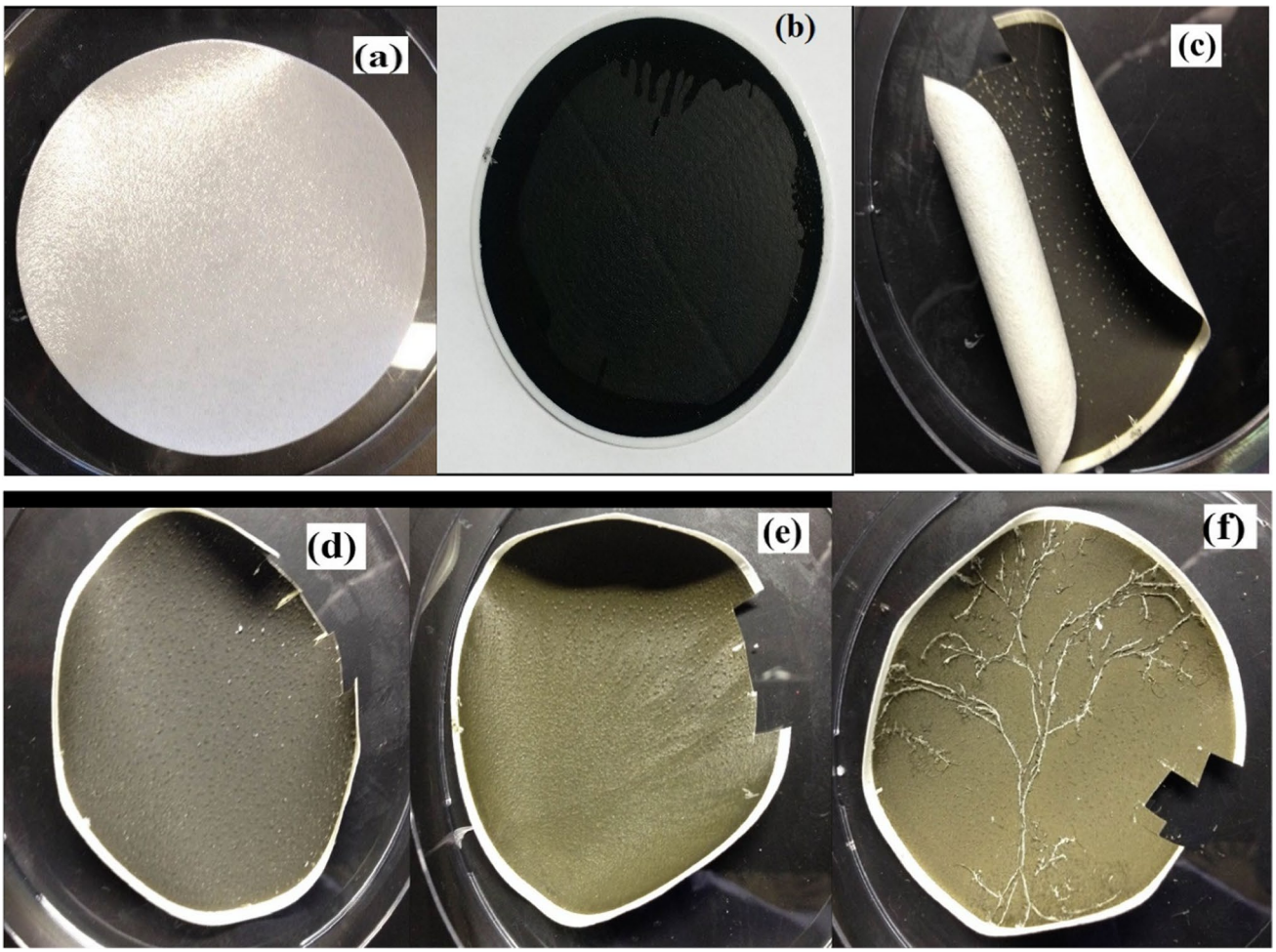

Fig. 3 Images of RC membrane surfaces **a** before and **b** after filtration before drying and dried membrane samples obtained from experimental conditions of **c** only Hg(II), **d** Hg + anions, **e** Hg + 0.2 mg/L HA, and **f** Hg + 1 mg/L HA, respectively

with HA gel-like materials were observed. When 1 mg/L HA was used, the surface was almost completely covered by the gel-like layer. The deposition of this layer is probably the cause of the increased flux decline observed when HA was present. The SEM images also show different morphology development on the membrane surface. There are many cube-like crystal particles present, which are similar to the major shapes of pyrite. When HA was present, there were also particles clusters observed. The difference in morphology of the particles is related to the interaction of Hg(II) and pyrite in presence of different chemicals. The particle clusters may be the result of linkage between complexes of Hg and thiol group in HA on the pyrite surface followed by formation of aggregated surface precipitates which might still preserve cube-like structure that is originated from pyrite [47, 48].

3.2 Stability of Hg/pyrite-deposited DE/UF system

The physical and chemical stability of Hg(II)-laden pyrite deposited on the membrane surface was evaluated using 0.1 M thiosulfate solutions, because thiosulfate has a strong affinity for mercury [2, 27]. The chemical stability was evaluated by detecting Hg in the permeate water after passing thiosulfate solution through the solids-laden membrane. Figure 5a shows that there were no substantial changes in flux for all cases during the stability tests, indicating that the thiosulfate solution did not affect the cake layers formed on the surface of membrane.

pH and Hg concentration were monitored over time during the stability experiments, and the results are shown in Fig. 5b and c. The effluent pH (Fig. 5b) varied between 7.5 and 6.8 for all experimental conditions, but the magnitude of

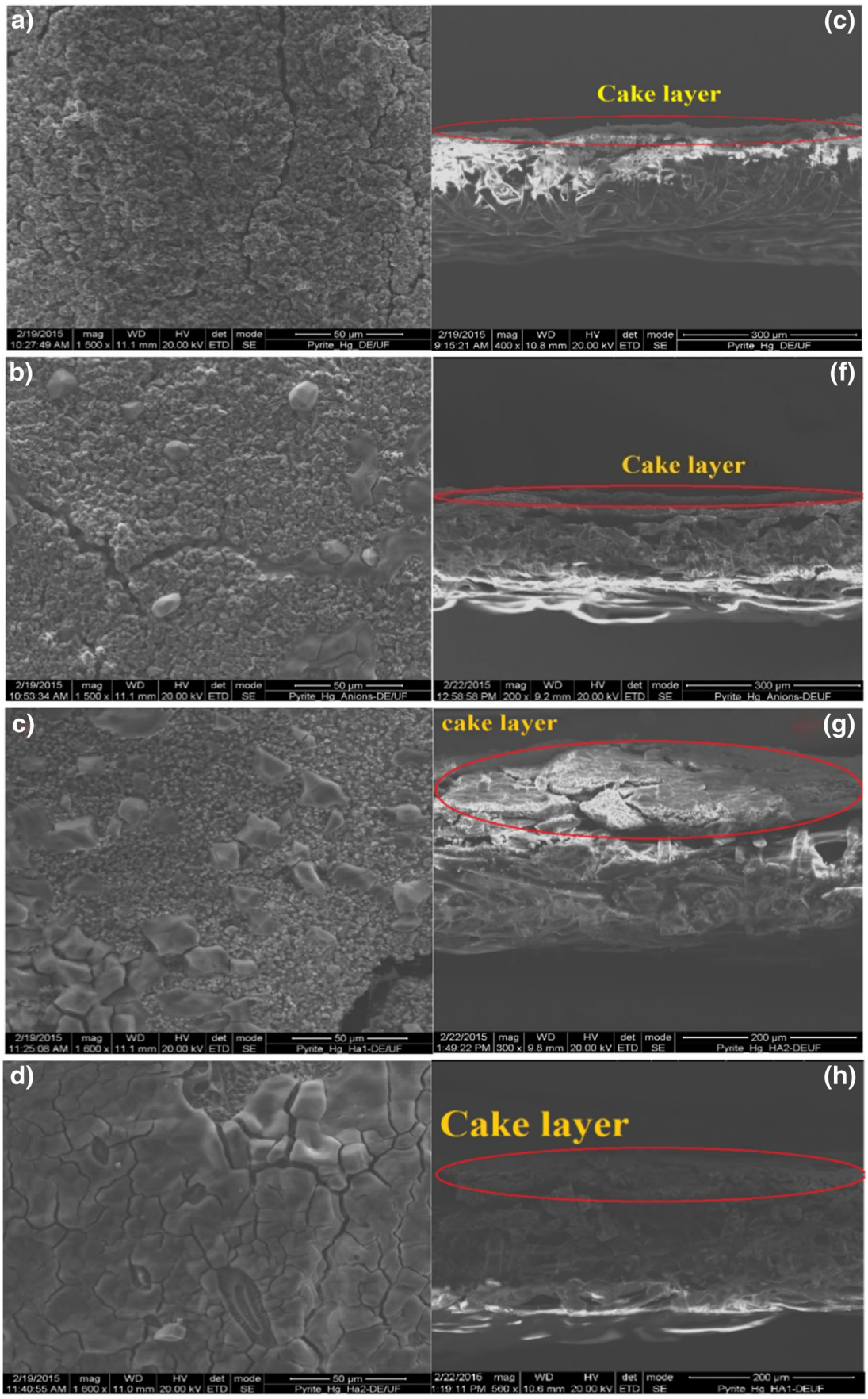

◂**Fig. 4** SEM images of RC membrane surfaces. Left side and right side show top view and cross sectional view of membranes for experimental conditions: **a**,**e** only Hg(II), **b**,**f** Hg + anions, **c**,**g** Hg + 0.2 mg/L HA, **d**,**h** Hg + 1 mg/L HA. Red circle denotes formation of cake layers. Conditions: pH 8, anoxic conditions under 14.5 psi pressure

change is much less than that observed during the rejection tests (Fig. 4). This change in pH may be due to the interaction of thiosulfate with the solid deposited on the membrane. Thiosulfate can be oxidized to tetrathionate by residual dissolved oxygen (Eq. (6)) or by iron (III) in the presence of pyrite [49]. Thiosulfate and tetrathionate can be decomposed to sulfate, bisulfide, and hydrogen ions via the disproportionation reactions shown in Eqs. (7)–(8):

$$2S_2O_3^{2-} + 0.5O_2 + 2H^+ \overset{\text{pyrite}}{\rightarrow} S_4O_6^{2-} + H_2O \quad (6)$$

$$S_2O_3^{2-} + H_2O = SO_4^{2-} + HS^- + H^+ \quad (7)$$

$$S_4O_6^{2-} + 12H_2O = 9SO_4^{2-} + 7HS^- + 17H^+ \quad (8)$$

Figure 5c shows that there was little Hg release after contact with thiosulfate, which means that the Hg-laden pyrite particles are very stable due to formation of highly insoluble precipitates or strong surface complexes. For comparison, Behra et al. (2001) [2] found that more than 89% of Hg was desorbed from Hg(II)-laden pyrite after 3 h of contact with 0.1 M thiosulfate solution at pH 7.1. Hyland et al. (1990) [27] also found around 90% desorption of Hg from the Hg(II)-laden pyrite after contact with 0.1 M thiosulfate at pH 6.7. The different level of Hg(II) desorption may be due to different experimental conditions and/or to different characteristics of the pyrite used in the different laboratories. Also, anoxic conditions were not secured during the experiments conducted by Behra (2001) [2] and Hyland (1990) [27]. Oxidation of the pyrite surface results in the formation of a monolayer of iron (oxyhydroxides) [47] that is less able to bind Hg(II) than pyrite. Also in their experiments, relatively large amounts of Hg were used in the adsorption tests compared to our experiments. Higher Hg loading on the pyrite surface might result in more weakly bound species.

The small amounts of mercury measured in the permeate water when HA was not present may be attributed to mixed physical and chemical adsorption mechanisms. The sorbed Hg species are desorbed by thiosulfate ligands, compared to other experimental conditions with anions or HA.

3.3 Recycle of Hg/pyrite-deposited UF membrane

To date, several experiments using pyrite-packed column tests [3] or regeneration/reuse of pyrite [4] have been attempted to investigate the ability of pyrite to further remove Hg(II). However, for such experiments, washing chemicals such as HCl or NaCl were used in both cases. The experiments for this study called recycle tests (step III in set I) were conducted to evaluate the residual capacity of pyrite to remove additional Hg after initial contact and removal by the UF membrane. This recycle experiment did not use a regenerant agent and only tested the continuous Hg(II) removal on the Hg(II)-pyrite-laden UF membrane surface. The motivation for this test is based on the hypothesis that complex chemical reactions of functional groups between Hg-HA-anion-S-(in-pyrite) can lead to another strong or stable chemical coordination [3].

Four feed solutions (Hg, Hg + anions, Hg + 0.2 mg/L HA, Hg + 1 mg/L HA) were prepared and fed to a DE/UF system that had previously been operated through steps I and II. The same operating conditions applied in the previous experiments were used. Figure 6a shows that flux was almost constant from the beginning to the end of the recycle test for all types of feed solutions. In the recycle test, the added feed solution appeared to pass through the membrane without making any physical impact on the cake layer. Figure 6b shows the change in pH with permeate volume per unit membrane area. Similar to the rejection tests, pH decreased to around 6 in all cases. Again, a smaller decrease in pH was observed in the case of Hg + anions, and a similar mechanism is applicable to explain the observations. In brief, the pH drop in the experiment with Hg only is due to adsorption of soluble mercury hydroxide species (Hg-OH) and associated release of protons. In the case of Hg + anions, formation of Hg-anion complexes (mostly Hg-Cl complex) reduces the free Hg to make complex with OH. But the effect of anions is not great. The dissociation of HA along with ternary surface complexes of pyrite-Hg-OH may attribute to the observed pH decrease.

Removal of Hg was nearly complete during these tests over the entire range of permeate volumes (1 L) evaluated in this study (Fig. 6c). These results indicate that this system is efficient for continuous and complete removal of Hg from water. It also indicates that it has the capacity to further remove Hg from contaminated waters after the pyrite particles are initially removed. Also, there was no significant release of Fe for all cases (Fig. 6d). These experimental results may support the hypothesis that a membrane filter containing pyrite-Hg(II) could provide another reactive cake layer capable of further removal of Hg(II) without post-chemical treatment for reuse. However, this can be only sustainably effective until flux decline is not severe due to the presence of NOM that shifts the cake layer formation to the pore blocking. That is, if NOM is separately pretreated from the influent water entering UF system, such pyrite-based UF treatment method may be effective in continuously removing Hg(II).

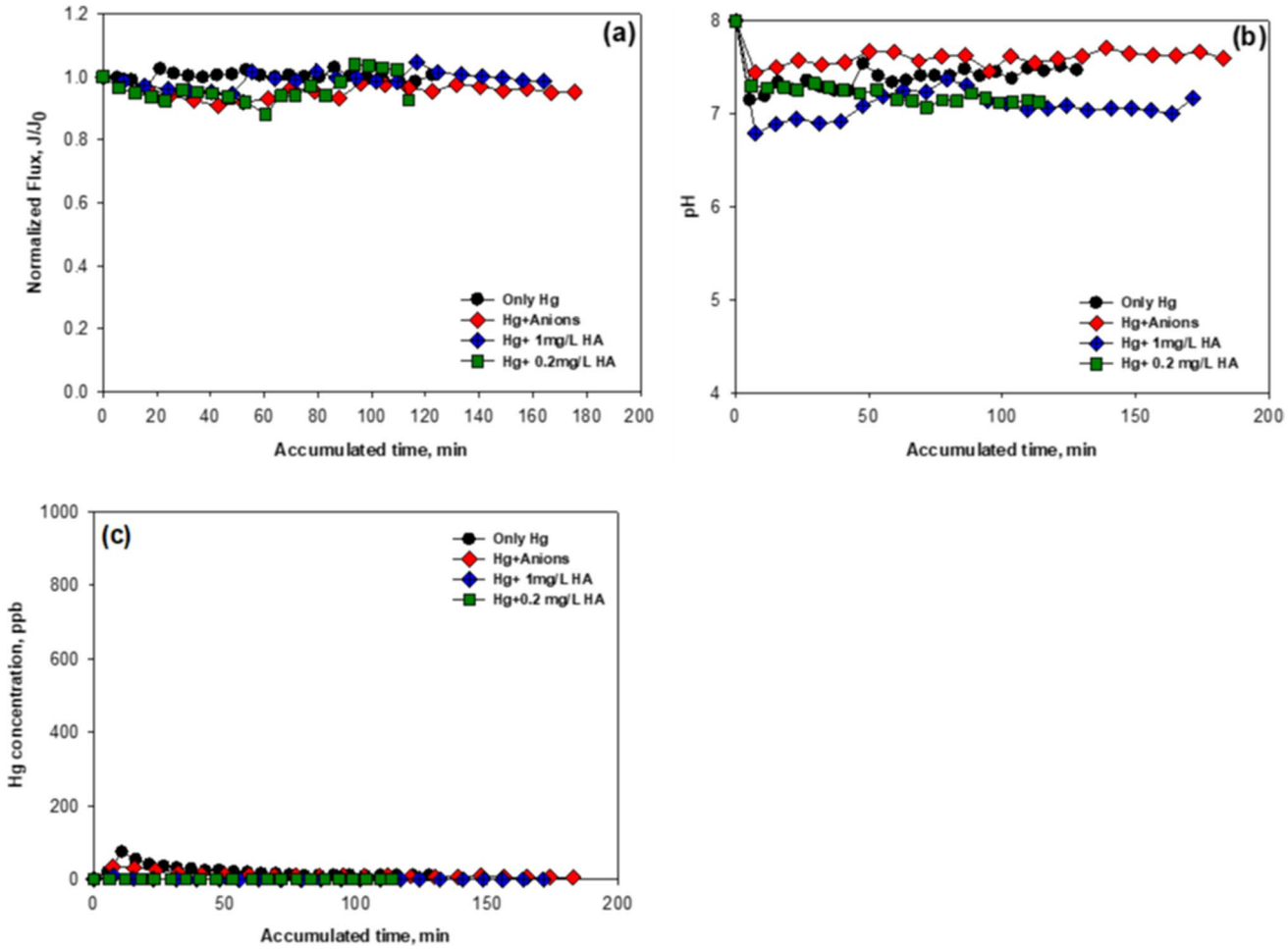

Fig. 5 **a** Flux decline of Hg(II), Hg(II)/anions, and Hg(II)/HA-contacted pyrite deposited on the membrane surface as fed by 0.1 M thiosulfate ($S_2O_3^{2-}$) solution; time-profiled **b** pH and **c** Hg in the same permeate water: 14.5 psi pressure, pH 8, and N_2-purged system

4 Conclusions

Due to strong tendency of the formation of stable solids (Hg-S-in-FeS_2), there have been many studies with a long journey to remove Hg(II) from solution using iron sulfides under various environmental conditions. However, there is still lack in evaluating the continuous removal capacity of pyrite in a filtration manner that does not require recollecting or retreatment after Hg(II) removal. This study tested the pyrite-supported UF system to investigate the ability of the continuous Hg(II) removal in the presence of co-existing ions and HA in terms of water flux, pH change, Hg(II) removal rate, and leaching of Fe contents.

Rejection experiments in the pyrite-supported UF system showed almost 100% removal of Hg(II), which indicates that it was nearly adsorbed onto pyrite and that the pyrite was nearly completely removed by the membrane. Nearly complete removal was observed even in the presence of anions or HA. Membrane fouling in all experiments could be ascribed to the formation of cake layers on the membrane surface. Even though insignificant amounts of Fe were observed in the permeate water, the possibility that HgS is formed via ion exchange between Hg(II) and Fe in the solid phase cannot be ruled out. It is possible that Fe is released from pyrite, but is re-adsorbed.

Desorption experiments using 0.1 M sodium thiosulfate ($Na_2S_2O_3$) solutions showed that adsorbed Hg(II) was not readily desorbed, indicating that Hg(II)-laden solids were stable. Although the effluent pH varied between 7.5 and 6.8 for all experimental conditions, but the magnitude of change is much less than that observed during the rejection tests. This change in pH may be due to the interaction of thiosulfate with the solid deposited on the membrane. However, detection of small amount of mercury in the permeate water for cases of only Hg(II) and Hg(II) + anions may be attributed to the mixed physical and chemical adsorption mechanisms. In recycle experiments, nearly complete Hg removal was observed and was maintained until the end of

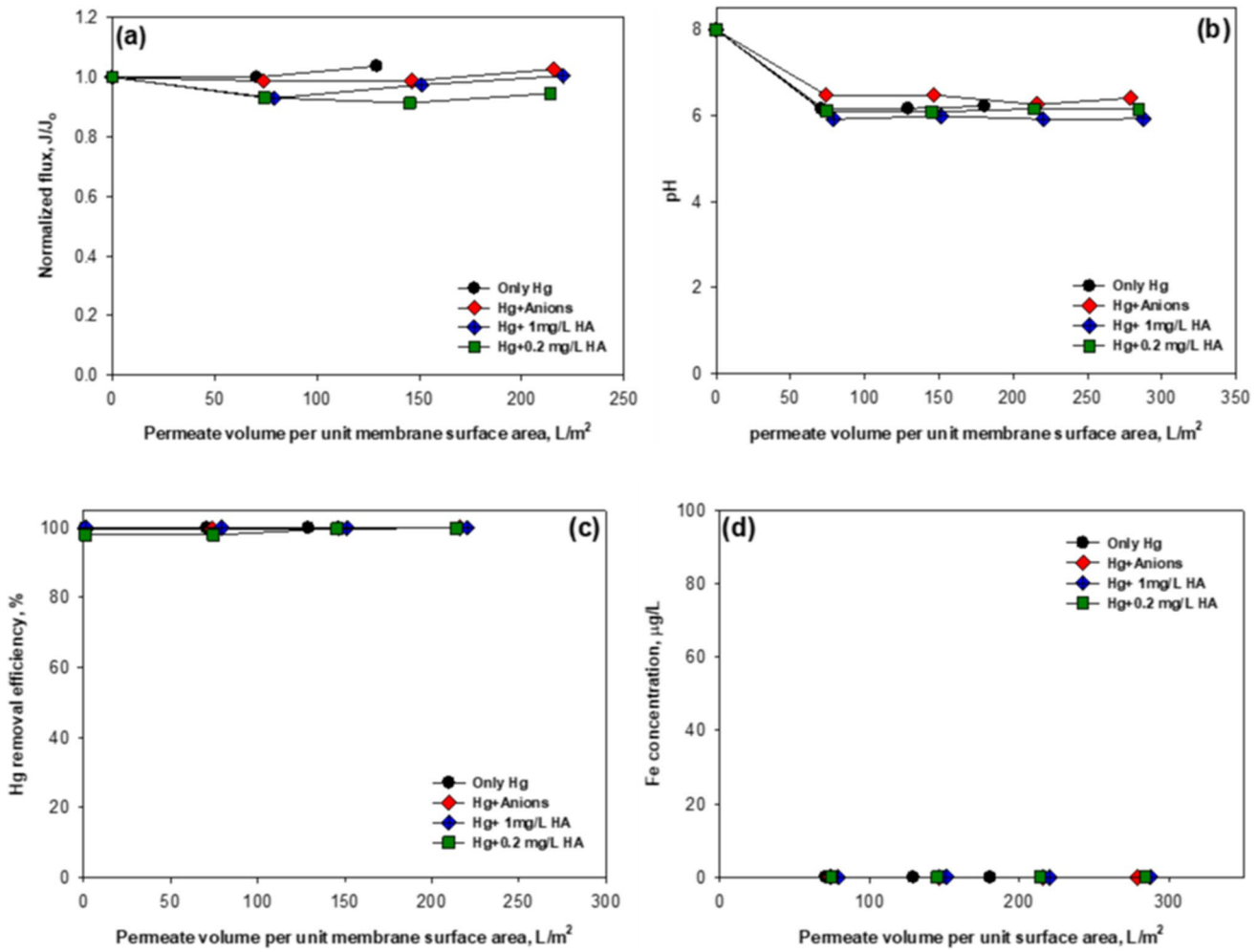

Fig. 6 Additional removal capacity of Hg-contacted pyrite laden on the UF membrane by providing continuous feed water containing 1 mg/L Hg(II), 10 mM anions (Cl^-, SO_4^{2-}, NO_3^-), 0.2 mg/L, or 1 mg/L HA at pH 8: **a** normalized flux, time profiled **b** pH, **c** Hg, and **d** Fe concentration

experiments, indicating that the pyrite retained additional capacity and that good Hg removal might be obtained with lower pyrite doses that were employed in these experiments.

The final goal of this study was to develop a treatment technology for continuous and complete removal of mercury from wastewater. The proposed reactive adsorbent membrane (RAM) hybrid process using dead-end ultrafiltration successfully demonstrated the continuous and almost complete removal of mercury from water. This study was tested in the absence of oxygen to clearly investigate how the reaction mechanism between Hg(II) and the unoxidized pyrite forms a stable solid and how the results obtained from the pyrite-supported UF system can contribute to continuous Hg(II) removal. This first set of experiments in our research plan will help to move smoothly to the next set of experiments in experimental conditions close to a real wastewater system containing various coexisting ions and oxygen. This gradual effort is expected to minimize the resulting data gap between laboratory batch testing and actual field application in Hg(II) removal using pyrite.

Supplementary Information The online version contains supplementary material available at https://doi.org/10.1007/s42247-021-00282-7.

Acknowledgements This publication was made possible by the National Priorities Research Program (NPRP) award [NPRP 4–279-2–094] from the Qatar National Research Fund (a member of The Qatar Foundation). The statements made herein are solely the responsibility of the authors. Open Access funding provided by the Qatar National Library.

References

1. H. Albatrni, H. Qiblawey, M.H. El-Naas, Comparative study between adsorption and membrane technologies for the removal of mercury. Sep. Purif. Technol. **257**, 117833 (2021)
2. P. Behra, P. Bonnissel-Gissinger, M. Alnot, R. Revel, J.J. Ehrhardt, XPS and XAS study of the sorption of Hg (II) onto pyrite. Langmuir **17**, 3970–3979 (2001)
3. J. Bower, K.S. Savage, B. Weinman, M.O. Barnett, W.P. Hamilton, W.F. Harper, Immobilization of mercury by pyrite (FeS_2). Environ. Pollut. **156**, 504–514 (2008)
4. Y. Sun, D. Lv, J. Zhou, X. Zhou, Z. Lou, S.A. Baig, X. Xu, Adsorption of mercury(II) from aqueous solutions using FeS and pyrite: a comparative study. Chemosphere **185**, 452–461 (2017)
5. M. Fayazi, Removal of mercury (II) from wastewater using a new and effective composite: sulfur-coated magnetic carbon nanotubes. Environ. Sci. Pollut. Res. **27**, 12270–12279 (2020)
6. H.Y. Jeong, B. Klaue, J.D. Blum, K.F. Hayes, Sorption of mercuric ion by synthetic nanocrystalline mackinawite (FeS). Environ. Sci. Technol. **41**, 7699–7705 (2007)
7. Y. Sun, Z. Lou, J. Yu, X. Zhou, D. Lv, J. Zhou, S.A. Baig, X. Xu, Immobilization of mercury (II) from aqueous solution using Al_2O_3-supported nanoscale FeS. Chem. Eng. J. **323**, 483–491 (2017)
8. Y. Duan, D.S. Han, B. Batchelor, A. Abdel-Wahab, Synthesis, characterization, and application of pyrite for removal of mercury. Colloids Surf. A Phys. Eng. Asp. **490**, 326–335 (2016)
9. D.S. Han, M. Orillano, A. Khodary, Y. Duan, B. Batchelor, A. Abdel-Wahab, Reactive iron sulfide (FeS)-supported ultrafiltration for removal of mercury (Hg (II)) from water. Water Res. **53**, 310–321 (2014)
10. D.S. Han, M. Orillano, Y. Duan, B. Batchelor, H. Park, N. Hilal, A. Abdel-Wahab, *Effect of Anions on Removal of Mercury (II) Using FeS-Supported Crossflow Ultrafiltration, Ultrafiltration: Methods, Applications and Insights* (Nova Science Publishers, Inc, 2017), pp. 129–152
11. L.Y. Blue, P. Jana, D.A. Atwood, Aqueous mercury precipitation with the synthetic dithiolate, BDTH2. Fuel **89**, 1326–1330 (2010)
12. S. Chiarle, M. Ratto, M. Rovatti, Mercury removal from water by ion exchange resins adsorption. Water Res. **34**, 2971–2978 (2000)
13. I. Wagner-Döbler, Pilot plant for bioremediation of mercury-containing industrial wastewater. Appl. Microbiol. Biotechnol. **62**, 124–133 (2003)
14. A. Johs, V.A. Eller, T.L. Mehlhorn, S.C. Brooks, D.P. Harper, M.A. Mayes, E.M. Pierce, M.J. Peterson, Dissolved organic matter reduces the effectiveness of sorbents for mercury removal. Sci. Total Environ. **690**, 410–416 (2019)
15 R. Melamed, F. Trigueiro, R. Villas Bôas, The effect of humic acid on mercury solubility and complexation. Appl. Organomet. Chem. **14**, 473–476 (2000)
16. P. Liang, Y.-C. Li, C. Zhang, S.-C. Wu, H.-J. Cui, S. Yu, M.H. Wong, Effects of salinity and humic acid on the sorption of Hg on Fe and Mn hydroxides. J. Hazard. Mater. **244**, 322–328 (2013)
17. U. Skyllberg, A. Drott, Competition between disordered iron sulfide and natural organic matter associated thiols for mercury (II)-An EXAFS study. Environ. Sci. Technol. **44**, 1254–1259 (2010)
18. M. Ravichandran, Interactions between mercury and dissolved organic matter—a review. Chemosphere **55**, 319–331 (2004)
19. Y. Duan, D.S. Han, B. Batchelor, A. Abdel-Wahab, Application of a reactive adsorbent-coated support system for removal of mercury (II). Colloids Surf. A: Phys. Eng. Asp. **509**, 623–630 (2016)
20. Z. Xiong, F. He, D. Zhao, M.O. Barnett, Immobilization of mercury in sediment using stabilized iron sulfide nanoparticles. Water Res. **43**, 5171–5179 (2009)
21. J.-J. Ehrhardt, P. Behra, P. Bonnissel-Gissinger, M. Alnot, XPS study of the sorption of Hg(II) onto pyrite FeS_2. Surf. Interface Anal. **30**, 269–272 (2000)
22. M. Svensson, B. Allard, A. Düker, Formation of HgS—mixing HgO or elemental Hg with S, FeS or FeS_2. Sci. Total Environ. **368**, 418–423 (2006)
23. A. Deonarine, H. Hsu-Kim, Precipitation of mercuric sulfide nanoparticles in NOM-containing water: Implications for the natural environment. Environ. Sci. Technol. **43**, 2368–2373 (2009)
24. Y. Yang, J. Liu, F. Liu, Z. Wang, S. Miao, Molecular-level insights into mercury removal mechanism by pyrite. J. Hazard. Mater. **344**, 104–112 (2018)
25. D.S. Han, J.K. Song, B. Batchelor, A. Abdel-Wahab, Removal of arsenite (As (III)) and arsenate (As (V)) by synthetic pyrite (FeS_2): synthesis, effect of contact time, and sorption/desorption envelopes. J. Colloid Interface Sci. **392**, 311–318 (2013)
26. D.S. Han, B. Batchelor, A. Abdel-Wahab, Sorption of selenium (IV) and selenium (VI) onto synthetic pyrite (FeS_2): Spectroscopic and microscopic analyses. J. Colloid Interface Sci. **368**, 496–504 (2012)
27. M. Hyland, G. Jean, G. Bancroft, XPS and AES studies of Hg (II) sorption and desorption reactions on sulphide minerals. Geochim. Cosmochim. Acta **54**, 1957–1967 (1990)
28. K.C. Gavilan, A. Pestov, H.M. Garcia, Y. Yatluk, J. Roussy, E. Guibal, Mercury sorption on a thiocarbamoyl derivative of chitosan. J. Hazard. Mater. **165**, 415–426 (2009)
29. N.J. O'Driscoll, E. Vost, E. Mann, S. Klapstein, R. Tordon, M. Lukeman, Mercury photoreduction and photooxidation in lakes: effects of filtration and dissolved organic carbon concentration. J. Environ. Sci. **68**, 151–159 (2018)
30. M. Haitzer, G.R. Aiken, J.N. Ryan, Binding of mercury (II) to aquatic humic substances: influence of pH and source of humic substances. Environ. Sci. Technol. **37**, 2436–2441 (2003)
31. B. Gu, Y. Bian, C.L. Miller, W. Dong, X. Jiang, L. Liang, Mercury reduction and complexation by natural organic matter in anoxic environments. Proc. Natl. Acad. Sci. **108**, 1479–1483 (2011)
32. K. Zheng, H. Li, L. Xu, S. Li, L. Wang, X. Wen, Q. Liu, The influence of humic acids on the weathering of pyrite: electrochemical mechanism and environmental implications. Environ. Pollut. **251**, 738–745 (2019)
33. M. Urgun-Demirtas, P.L. Benda, P.S. Gillenwater, M.C. Negri, H. Xiong, S.W. Snyder, Achieving very low mercury levels in refinery wastewater by membrane filtration. J. Hazard. Mater. **215**, 98–107 (2012)
34. I. Makertihartha, Z. Rizki, M. Zunita, P.T. Dharmawijaya, Graphene based nanofiltration for mercury removal from aqueous solutions. Adv. Sci. Lett. **23**, 5684–5686 (2017)
35. M. Mullett, L. Mohamed, Removal of mercury from solution using reverse osmosis filtration, Engineering Our Future: Are We up to the Challenge?: 27–30 September 2009, Burswood Entertainment Complex, 2207 (2009)
36. M. Yaqub, S.H. Lee, Micellar enhanced ultrafiltration (MEUF) of mercury-contaminated wastewater: Experimental and artificial neural network modeling. J. Water Process Eng. **33**, 101 (2020)

37. E.J. Kim, B. Batchelor, Synthesis and characterization of pyrite (FeS_2) using microwave irradiation. Mater. Res. Bull. **44**, 1553–1558 (2009)
38. D. Wei, K. Osseo-Asare, Aqueous synthesis of finely divided pyrite particles. Colloids Surf. A: Phys. Eng. Asp. **121**, 27–36 (1997)
39. D. Obrist, J.L. Kirk, L. Zhang, E.M. Sunderland, M. Jiskra, N.E. Selin, A review of global environmental mercury processes in response to human and natural perturbations: changes of emissions, climate, and land use. Ambio **47**, 116–140 (2018)
40. P. Ačai, E. Sorrenti, T. Gorner, M. Polakovič, M. Kongolo, P. de Donato, Pyrite passivation by humic acid investigated by inverse liquid chromatography. Colloids Surf. A: Phys. Eng. Asp. **337**, 39–46 (2009)
41. A. Jawor, E.M. Hoek, Removing cadmium ions from water via nanoparticle-enhanced ultrafiltration. Environ. Sci. Technol. **44**, 2570–2576 (2010)
42. S. Wu, X. Hua, B. Ma, H. Fan, R. Miao, M. Ulbricht, C. Hu, J. Qu, Three-dimensional analysis of the natural-organic-matter distribution in the cake layer to precisely reveal ultrafiltration fouling mechanisms. Environ. Sci. Technol. **55**, 5442–5452 (2021)
43. S. Hong, M. Elimelech, Chemical and physical aspects of natural organic matter (NOM) fouling of nanofiltration membranes. J. Membr. Sci. **132**, 159–181 (1997)
44. A. Schäfer, A.G. Fane, T. Waite, Fouling effects on rejection in the membrane filtration of natural waters. Desalination **131**, 215–224 (2000)
45. M. Kumar, H.M. Baniowda, N. Sreedhar, E. Curcio, H.A. Arafat, Fouling resistant, high flux, charge tunable hybrid ultrafiltration membranes using polymer chains grafted graphene oxide for NOM removal. Chem. Eng. J. **408**, 127300 (2021)
46. J.D. Rimstidt, D.J. Vaughan, Pyrite oxidation: a state-of-the-art assessment of the reaction mechanism. Geochim. Cosmochim. Acta **67**, 873–880 (2003)
47. A. Manceau, C. Lemouchi, M. Enescu, A.-C. Gaillot, M. Lanson, V. Magnin, P. Glatzel, B.A. Poulin, J.N. Ryan, G.R. Aiken, Formation of mercury sulfide from Hg (II)–thiolate complexes in natural organic matter. Environ. Sci. Technol. **49**, 9787–9796 (2015)
48. U. Skyllberg, A. Persson, I. Tjerngren, R.-M. Kronberg, A. Drott, M. Meili, E. Björn, Chemical speciation of mercury, sulfur and iron in a dystrophic boreal lake sediment, as controlled by the formation of mackinawite and framboidal pyrite. Geochim. Cosmochim. Acta. **294**, 106–125 (2021)
49. Y. Xu, M.A. Schoonen, The stability of thiosulfate in the presence of pyrite in low-temperature aqueous solutions. Geochim. Cosmochim. Acta **59**, 4605–4622 (1995)